Journal of Global Positioning Systems (2025)
Vol. 21, Issue 2: 124-138
DOI:10.5081/jgps.21.2.124

Analysis of the influence of strong magnetic storms on precise point positioning in China

Wei Xiang[1] Xiaomin Luo[1] Zhuang Chen[1] Biyan Chen[3]
Ankang Xie[1] Lingqiao Zeng[1] Yingrui Wang[1] Kamarul Hawari Bin Ghazali[2,4]

1) China University of Geosciences, School of Geography and Information Engineering, Wuhan, 430079, China
2) Joint International Research Laboratory of Spatio-temporal Information and Intelligent Location Services, Guilin University of Electronic Technology, Guilin 541004, China
3) School of Geoscience and Info-physics, Central South University, Changsha 410083, China
4) Center for Advanced Industrial Technology, University Malaysia Pahang Al Sultan Abdullah, Pekan 26600, Malaysia

Corresponding author, Xiaomin Luo luoxiaomin@cug.edu.cn

Abstract: It is currently in the active period of the 25th solar cycle, and magnetic storm events occur frequently. To study the impact of magnetic storms on precise point positioning (PPP) in China, PPP experiments were carried out using 17 IGS stations data in China based on a total of 84 strong magnetic storm events from 2000 to 2024. The rate of total electron content index (ROTI) and the detrended total electron content (dTEC) were used to reflect the impact of magnetic storms on the ionosphere over the 17 stations. GNSS PPP positioning accuracy of magnetic static days and magnetic storm days was compared and analyzed. Meanwhile, the cluster analysis method was introduced to investigate the correlation between GNSS positioning accuracy and latitude during magnetic storms. Experimental results show that 50%-60% of strong magnetic storms do not significantly impact the GNSS PPP positioning accuracy and regional ionospheric environment of these IGS stations in China. The ionosphere in the low-latitude region of China is more sensitive to magnetic storms, and in the strong magnetic storm environment, the ROTI index can reach 4 TECU/min, the ambiguity resolved percentage decreases significantly, and the GNSS PPP 3D error can reach several meters. GNSS stations in the mid-latitude region can show relatively stable PPP positioning results in the magnetic storm environment, and more than 90% of the magnetic storms do not cause obvious positioning errors in the mid-latitude stations.

Keywords: Geomagnetic storm; Ionosphere; Precise point positioning; Positioning accuracy; Ionospheric disturbance

1 Introduction

Precise point positioning (PPP) technology is based on precision products such as precise orbit and clock products, and utilizes pseudorange and carrier phase observations from a single global navigation positioning receiver to achieve high-precision positioning through an undifferenced method (Zumberge et al., 1997). Global navigation satellite systems (GNSS), including GPS (USA), Galileo (EU), GLONASS (Russia), and BeiDou (China), have been continuously advancing. This has led to significant breakthroughs in PPP technology, enabling positioning accuracy to reach the centimeter or even millimeter level (Zhang et al., 2015).

The current solar activity cycle (Solar Cycle 25) commenced in December 2019, with its maximum

Editor-In-Charge: Dr. Xingxing Li

activity projected around 2025–2026. An initial peak occurred in late 2022, with a second maximum anticipated between June 2025 and mid-2026 (Wang et al., 2025). During solar maximum, the frequency of solar flares and coronal mass ejections (CMEs) increases significantly. These violent solar activities can release a large number of high-energy particles and enhanced solar wind to the Earth (Gonzalez et al., 1994; Luo et al., 2022), which interact with the Earth's magnetic field and cause geomagnetic storms. Under geomagnetic storm conditions, rapid changes in the magnetospheric electric field cause drastic alterations in ionospheric parameters such as plasma density, temperature, and electric field (Polekh et al., 2022). This leads to irregular variations in the ionospheric electron content, thereby inducing ionospheric disturbances, which in turn affect the performance of GNSS PPP (Astafyeva et al., 2014; Luo et al., 2025).

Luo et al. (2023) evaluated the positioning performance under 67 geomagnetic storms of varying intensities that occurred over the five-year period from 2018 to 2022, and the results indicated that during strong storms, the PPP ambiguity resolved percentage of global GNSS stations are generally lower than 90.0%, especially for the PPP ambiguity resolved percentage of some stations located at low latitudes which are lower than 40.0%. Filjar et al. (2008) analyzed the positioning performance of the Osijek reference station in Croatia from October 13 to November 3, 2003, and revealed that during geomagnetic storms, the height and north components of GPS positioning errors were significantly affected, whereas the east component was barely impacted. Quan et al. (2021) studied the GPS single-frequency point positioning performance during the main phase of different types of geomagnetic storms, indicating that the probability of extreme positioning errors is higher during intense geomagnetic storm main phases, and the positioning accuracy in the U-direction was significantly more affected than in other directions. Furthermore, the positioning accuracy may also be notably impacted during the recovery phase of geomagnetic storms. Wang et al. (2021) focused on the geomagnetic storm event on August 26, 2018, and analyzed the ionospheric response in high-latitude regions of the Northern Hemisphere and its impact on GNSS PPP. The results indicated that during the occurrence of scintillations, the positioning errors of all stations increased significantly, with the horizontal and vertical positioning errors increasing to approximately 0.9 m and 1.7 m, respectively. Sang et al. (2023) analyzed the abnormal variations in the ionospheric total electron content and the GPS positioning performance over the Northern Hemisphere caused by the geomagnetic storm event on August 26, 2018, based on IGS global observation data and Global Ionospheric Maps (GIMs). The results indicated that during the geomagnetic storm, the cycle slip variations in the observation data from high-latitude regions were significant, with the cycle slip ratio decreasing by a maximum of 61.84% compared to geomagnetically quiet days. Additionally, the data completeness rate of all stations declined during the storm, among which the decrease was faster and more severe in high-latitude regions (reaching 38.65%), accompanied by a significant increase in positioning errors. Zakharenkova et al. (2021) analyzed observation data from over 4500 ground-based GPS stations in the United States during the intense geomagnetic storm on September 7-8, 2017, and found that during geomagnetic storms, the 3D positioning errors of stations affected by Equatorial Plasma Bubbles (EPBs) in the low to middle latitudes of North America increased to several meters, with errors even exceeding 5 meters at some stations, and the error distribution was highly consistent with the expansion path of EPBs. Li et al. (2023) constructed a grid-based polynomial fitting and residual interpolation model, considering the impacts of reference station distribution, satellite elevation angle, and the Rate of Total Electron Content Index (ROTI). During the ionospheric active period, this approach improved the average horizontal positioning accuracy of precise point positioning real-time kinematic (PPP-RTK) from the decimeter level to the centimeter level, and the ambiguity fixing rate also increased from 80.6% to 90.0%. Zhang et al. (2025)

found that ionospheric scintillation tends to result in inaccurate estimation of ionospheric uncertainty. Consequently, they proposed that users acquire ionospheric scintillation information from the server to optimize their positioning strategies, thereby improving the positioning accuracy of real-time kinematic (RTK). During the period of optimal effectiveness, the positioning error can be reduced by approximately 50%. Li et al. (2025) proposed two novel ionospheric scintillation parameters, namely the Standard Deviation of Time-Difference Phase Ionospheric Residual (SOT) and the Standard Deviation of Double-Differenced Triple-Frequency Phase Residual (SOD). Effectiveness analysis was conducted using SOT, SOD, ROTI, and σ_{φ}. Experimental results indicated that the correlation coefficient between SOT and σ_{φ} reached 0.957, while SOD was highly correlated with σ_{φ}. Both parameters could effectively capture the scintillation intensity and spatial distribution. Li et al. (2025) addressed the adverse impacts of ionospheric scintillation on PPP-RTK technique in low-latitude regions. They improved the algorithm model from both the server side and the user side, optimizing the processes of cycle-slip detection, ionospheric uncertainty characterization, and observation calibration. Experimental results demonstrated that, validated with data from 10 stations in the Hong Kong network, the improved method could still achieve a positioning accuracy of less than 2 cm in the horizontal direction and less than 4 cm in the vertical direction under strong scintillation conditions. Compared with the conventional PPP-RTK solution, the positioning accuracy is improved by up to 50%–80%. Existing studies have primarily focused on specific geomagnetic storm events or those occurring within short time periods, analyzing the impact of geomagnetic storms on PPP under specific conditions, with a predominant emphasis on high-latitudes or low-latitudes regions.

Currently, we are in the active phase of the 25th solar cycle, approaching the second peak of this cycle (Wang et al., 2025). To investigate the actual impact of geomagnetic storms on PPP in China region, this study analyzes strong geomagnetic storms with a minimum Dst index of less than -100 nT, based on geomagnetic data from 2000 to 2024. Utilizing data from 17 International GNSS Service (IGS) global tracking stations within China, it examines the effects of geomagnetic storms on PPP at and around these stations in China. Meanwhile, a cluster analysis algorithm is adopted to explore the correlation between positioning disturbances and latitude during geomagnetic storms. This research is expected to provide a reference for users of GNSS precise positioning in China under geomagnetic storm conditions.

2 Data and Methods

2.1 Selection of Magnetic Storm Events and GNSS Stations

The experimental data in this study are derived from the IGS network. The observation stations selected are 17 IGS continuous tracking stations located within China. Over the time scale from 2000 to 2024, to ensure that the acquired data contain relatively complete observation signals, we finally recorded a total of 84 major magnetic storm events, and the research is conducted with the day when the minimum Dst value of each magnetic storm occurs as the magnetic storm day. The timing of geomagnetic storm events and the Dst index are shown in Figure 1.

For these 84 magnetic storm events, the observation data from 17 tracking stations in China were downloaded sequentially from the IGS network. The distribution of these stations is shown in Figure 2. The available data information of each station during strong geomagnetic storm events is presented in Figure 3. The vertical axis represents the serial number of magnetic storm events. Meanwhile, Figure 3 also displays the receiver information of each station, which is distinguished by different colors.

2.2 Rate of Total Electron content Index

Geomagnetic storms induce anomalous ionospheric disturbances by altering ionospheric electron density, thereby affecting the positioning accuracy of PPP through factors such as ionospheric delay errors and scintillations.

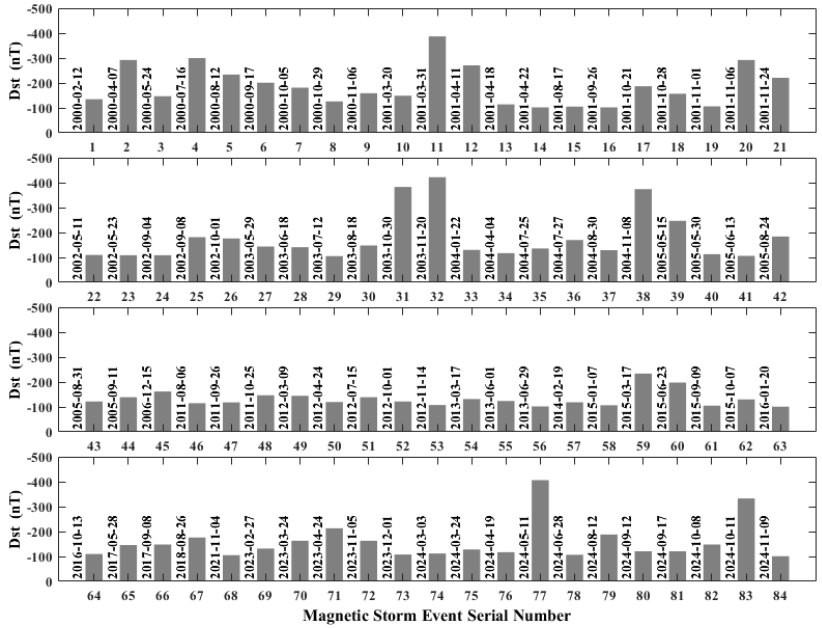

Figure 1 Timing of magnetic storm events and their Dst indices

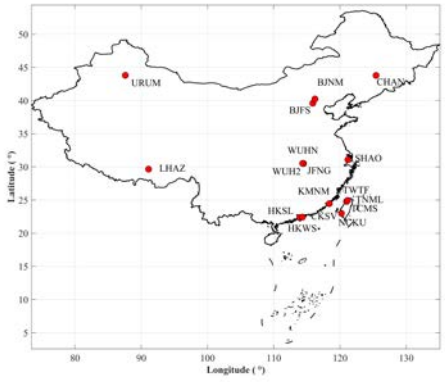

Figure 2 Geographical distribution of the 17 IGS stations

The ROTI is a quantitative indicator characterizing variations in Total Electron Content (TEC), which can be used to quantify the severity of ionospheric disturbance impact on carrier phase measurements. The calculation method of ROTI is as follows (Pi et al., 1997):

$$ROTI = \sqrt{< ROT^2 > - < ROT >^2} \qquad (1)$$

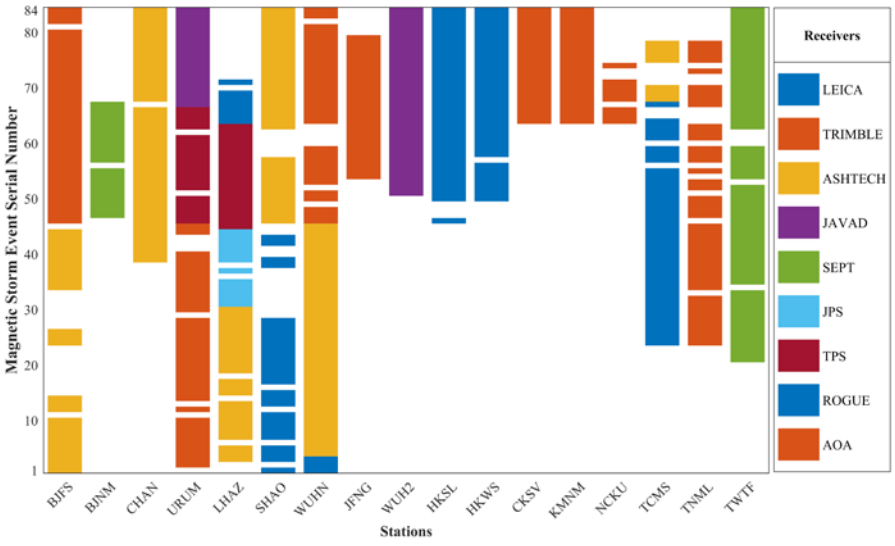

Figure 3 Data availability and receivers of each station during geomagnetic storm events

wherein the $<>$ denotes the average value within a time interval. For GNSS observations with a sampling rate of 30 seconds, the time window is typically set as 5 minutes. ROT represents the rate of change of TEC, with the unit being TECU per minute. The formula for calculating ROT using GPS observation data with a 30 second sampling interval is as follows (Cherniak et al., 2018):

$$ROT = \frac{STEC_k^i - STEC_{k-1}^i}{t_k - t_{k-1}} = \frac{f_1 f_2 \cdot (f_2 \Delta L_1 - f_1 \Delta L_2) \cdot c}{K \cdot \left(f_1^{\,2} - f_2^{\,2}\right) \cdot \Delta t} \quad (2)$$

In this formula, i and k denote the GPS satellite and epoch, respectively; Δ represents the difference operation between adjacent epochs; f_1 and f_2 correspond to the carrier frequencies of different signals, where $f_1 = 1575.42$ MHz and $f_2 = 1227.60$ MHz. L_1 and L_2 are the phase observations of GPS at the two distinct frequencies, with the unit of cycle; K=40.3 × 10^{16} m^3/s^2; c is the speed of light, with c=299792458 m/s; and $STEC$ denotes the slant total electron content.

The ROTI index can effectively characterize GPS phase fluctuations, detect ionospheric irregularities, and identify regions with anomalous variations in electron density within the ionosphere. By analyzing changes in ROTI during geomagnetic storms, the dynamic evolution of the ionosphere under the influence of such storms can be elucidated.

2.3 Detrended Total Electron Content

Using dual-frequency GPS carrier phase observations, the slant ionospheric electron content along the signal propagation path from each satellite to the receiver can be calculated (Tang et al., 2018):

$$STEC = \frac{1}{40.3 \times 10^{16}} \frac{f_1^2 f_2^2}{f_1^2 - f_2^2} (L_1 - L_2 + const + \varepsilon) \quad (3)$$

where $STEC$ denotes the ionospheric TEC with the unit of TECU; L_1 and L_2 are the carrier phase observations; f_1 and f_2 are the carrier phase frequencies; const is the unknown constant bias, including errors such as carrier phase integer ambiguity and instrumental bias; and ε represents the noise during measurement. To eliminate the background trend and unknown constant bias in the TEC time series, the Savitzky-Golay smoothing filter is used to fit the observed TEC time series.

$$\overline{STEC}(t) = \sum_{i=-m}^{n} a_i STEC(t+i) \quad (4)$$

In the formula, $\overline{STEC}(t)$ is the fitted TEC at the observation epoch *t*; *m* and *n* represent the moments before and after the data point at epoch t, respectively; the length of the moving window is (*m*+*n*+1), and in this paper, the length of the moving window is set to 121; and a_i denotes the filter coefficient.

The detrended total electron content time series can be obtained by subtracting the fitted TEC time series from the observed TEC time series.

$$dTEC(t) = STEC(t) - \overline{STEC}(t) \quad (5)$$

In the formula, $dTEC(t)$ denotes the detrended TEC at epoch t. The dTEC reflects the real-time variation of ionospheric electron density and can accurately represent the ionospheric disturbances induced by abnormal events. By monitoring the changes in dTEC, the impact of ionospheric disturbances on satellite communication and navigation positioning can be analyzed, which ensures the stable operation of communication and navigation systems.

2.4 K-means cluster analysis

Cluster analysis is an unsupervised classification method that categorizes samples based on their similarity. For a given dataset and a preset number of clusters, the K-means clustering method iteratively optimizes to partition the data into non-overlapping clusters, maximizing the similarity of data within the same cluster and minimizing the similarity of data between different clusters. K-means takes the minimization of the within-cluster sum of squares as the optimization objective, and its calculation formula is shown in Equation (6):

$$P = \sum_{i=1}^{K} \sum_{x \in C_i} d^2\left(x_j, \bar{x}_i\right) \quad (6)$$

In the formula, P denotes the sum of squared distances between all elements in the K clusters and the centroid of their respective clusters after clustering; C_i represents the i-th cluster; $d(a,b)$is

used to calculate the Euclidean distance between two points; and $\bar{x}_i$ denotes the centroid of the i-th cluster.

2.5 Positioning Strategy

In this study, the open-source software PRIDE PPP-AR developed by Wuhan University (Geng et al., 2019, 2022) is used for PPP, with the positioning mode being kinematic PPP The carrier phase and pseudorange observations of GPS L1 and L2 frequencies are involved in the solution. The parameter configuration basically adopts the default settings. The parameter configuration of PRIDE PPP-AR is shown in Table 1. For the precise products used in the solution (including precise ephemeris, precise clock offsets, Earth rotation parameter files, quaternion products, and bias products) are all adopted from those released by the Center for Orbit Determination in Europe (CODE). are used for the period from 2000 to 2020. During the positioning process, the satellite cutoff elevation angle is set to 7°. The ionosphere is corrected using the ionosphere-free model, and the troposphere is processed with the Global Pressure and Temperature (GPT) model and Global Mapping Functions (GMF). Meanwhile, ambiguity resolution is assisted by fixed solutions, with the ambiguity fixing method being the rounding method. Regarding the processing details, this study follows the default configurations specified in the PRIDE PPP-AR documentation. For more relevant information, please visit the official website of PRIDE LAB (https://pride.whu.edu.cn/).

Table 1 Parameter table of PRIDE PPP-AR

Item	Atrategies
GNSS system	GPS
Observations	Pseudorange and carrier phase
Frequency	L1 and L2
Cut off angle	7 degrees
Interval	30 seconds
PPP model	Kinematic
Precise products	CODE products (sp3; clk; erp; bia; obx)
Ambiguity	Fixed solution

3 Results Analysis and Discussion

3.1 Overall Analysis of the Impact of Magnetic Storms on Station Positioning

The observation data are processed using PRIDE PPP-AR for kinematic PPP. Simultaneously, the ROTI and dTEC indices are calculated using the observation data and ephemeris files to characterize the ionospheric activity over the stations during magnetic storms. The fluctuations in ROTI and dTEC are used to determine whether the stations are disturbed by magnetic storms during positioning, while the positioning results are analyzed to evaluate the degree of accuracy degradation caused by such disturbances.

For the analysis of positioning accuracy, only the deviations induced by magnetic storms are considered. For cases where significant positioning errors occur without magnetic storm influence, referring to the fact that such errors also exist during geomagnetically quiet periods, they are attributed to other factors such as the positioning environment - including multipath effect interference and tropospheric error interference—rather than magnetic storms.

The statistical results of ionospheric disturbances and positioning perturbations during magnetic storms are presented in Figure 4. "Minor ionospheric disturbances" refers to slight fluctuations in ionospheric indices of only a small subset of epochs and satellites compared to the quiet period in January 2019, with the fluctuation amplitude not exceeding the upper limit of natural fluctuations during the quiet period. "Significant ionospheric disturbances" indicates enhanced ionospheric irregularities caused by magnetic storms, characterized by synchronous and obvious fluctuations in ionospheric indices across widespread epochs and multiple satellites, with values significantly higher than those during the quiet period. "Minor positioning disturbances" means that although the positioning accuracy fluctuates compared to the quiet period, the three-dimensional error still remains within the centimeter-level range, which can meet the needs of general high-precision applications. "Significant positioning disturbances" is affected by the significant ionospheric disturbance induced by

magnetic storms, leading to a substantial degradation of positioning accuracy. The 3D error exceeds the threshold for centimeter-level applications, making it unable to meet the requirements of precise positioning. As can be seen from the figure, for most magnetic storm events, the IGS tracking stations in the China region do not show severe disturbance, especially those stations in mid-latitude areas. However, under extremely severe magnetic storm conditions, the ionosphere undergoes intense disturbances, and the positioning accuracy of each station will exhibit significant fluctuations that vary with the ionospheric conditions. Figure 5 shows the thermal distribution of 3D root mean square error (RMS) values of each station across different value ranges (upper subplot) and the thermal distribution of maximum 3D positioning error values of each station across different value ranges (lower subplot).

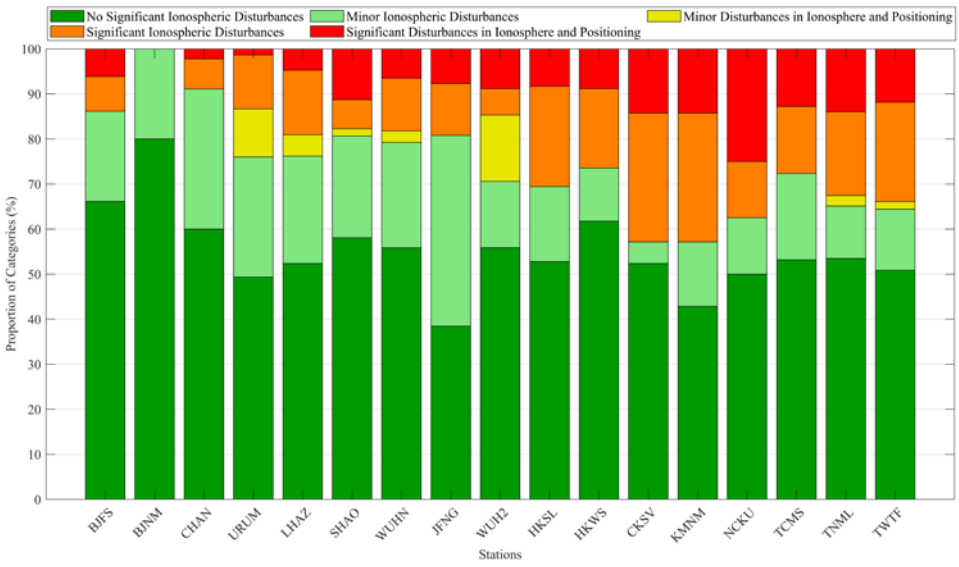

Figure 4 Impact of magnetic storms on each station

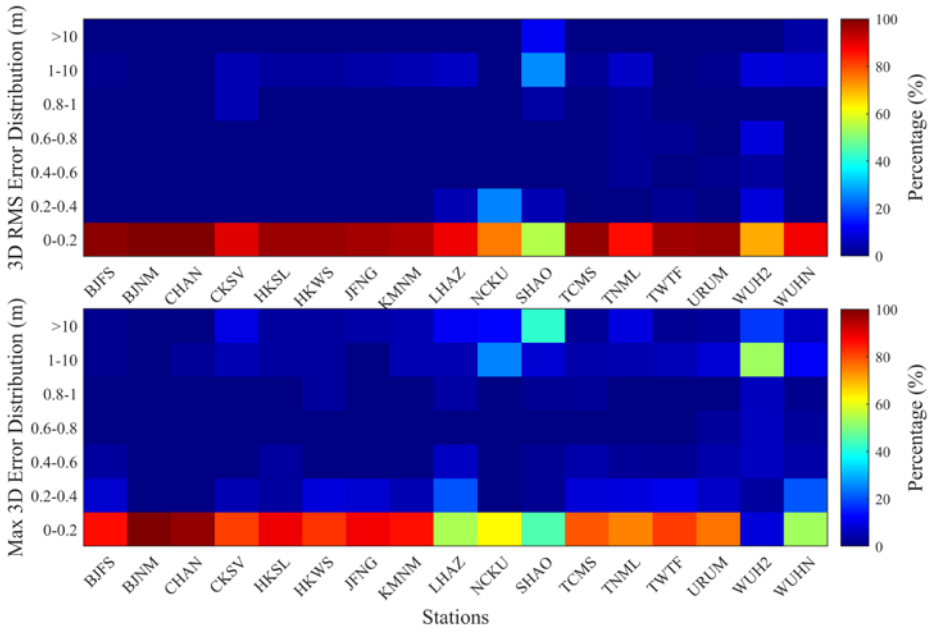

Figure 5 Thermal distribution map of error statistics for each station

Based on Figures 4 and 5, the 17 IGS stations distributed within China's territory are divided into four major regions: the mid-latitude region of northern China, the western region of China, the

central region of China, and the low-latitude region of southern China. Each of these regions is discussed individually.

In the mid-latitude region of northern China, there are two IGS tracking stations in the Beijing area, namely BJFS and BJNM. Over the years, magnetic storms have rarely caused severe effects on the ionospheric environment in the Beijing area, and the vast majority of magnetic storms have not exerted significant effects on positioning. Under extreme conditions, the fluctuation range of positioning errors of GPS PPP has remained within 0.5 meters. Consistent with BJNM, the CHAN station, also situated in the mid-latitude zone, has barely been significantly affected by geomagnetic storms:

In western China, there are two IGS stations, namely URUM in Urumqi and LHAZ in Lhasa. Possibly constrained by environmental factors, both stations exhibit significant error perturbations even without geomagnetic storm interference. Under geomagnetic storm conditions, the URUM station is relatively less affected by intense ionospheric disturbances induced by strong geomagnetic storms, but minor ionospheric disturbances occur relatively frequently, accompanied by slight error fluctuations in some epochs. The positioning errors are small, and the duration of positioning perturbations is short. For the LHAZ station, the ROTI values of multiple satellites are relatively high, reaching 2–3 TECU/min. However, the impact of geomagnetic storms on the PPP positioning of this station is not obvious, with most storm-induced positioning perturbations not exceeding 0.3 meters. Only during a geomagnetic storm in September 2002 did obvious and intense abnormal perturbations occur, with errors ranging from several meters to tens of meters.

The IGS stations in central China are primarily distributed in Wuhan and Shanghai. Among these, the SHAO station in Shanghai (31.1°N) exhibited relatively poor positioning performance under the influence of geomagnetic storm events from 2000 to 2024, with frequent abnormal perturbations in certain epochs and overall low positioning quality. Additionally, fluctuations in the ROTI and dTEC induced by magnetic storms are also significant. The ROTI value can occasionally reach 4 TECU, leading to obvious ionospheric disturbances, and the resulting positioning errors can reach several meters. The WUHN, WUH2, and JFNG stations in Wuhan are situated at a latitude of approximately 30.5°N. For the WUHN station, while most geomagnetic storms were accompanied by intense ionospheric disturbances, the occurrence probability of such disturbances was relatively low at only 18% when considering the entire dataset. Regarding positioning accuracy under abnormal conditions, the errors generally did not exceed 0.5 meters, with extreme errors around 1–2 meters. The other two IGS stations in Wuhan (WUH2 and JFNG) displayed essentially identical positioning characteristics to WUHN: the ionospheric environment remained generally stable, positioning perturbations were relatively slight, most errors were within 0.5 meters, and extreme errors were approximately 1–2 meters. Particularly, even when the ionosphere is not affected by magnetic storms, the WUH2 station still exhibits significant positioning error anomalies in some epochs, which consequently leads to abnormalities in its error thermal distribution map.

Hong Kong and Taiwan of China are representative low-latitude regions in the country. The IGS has two stations in Hong Kong, namely HKSL and HKWS, and six continuous tracking stations in Taiwan, including KMNM, CKSV, TCMS, TNML, TWTF, and NCKU. In the Hong Kong region, magnetic storms can cause relatively intense ionospheric disturbances, which in turn lead to severe positioning perturbations. In severe cases, phenomena such as GPS satellite signal loss of lock and a reduction in the number of available satellites may occur. When positioning is performed using PRIDE PPP-AR, the positioning error ranges from 0.3 to 0.4 meters; In extremely harsh positioning environments, the positioning error can reach several meters or even tens of meters. In Taiwan, another low-latitude region, during historical magnetic storm events, the ionospheric interference caused by magnetic storms in this area was relatively obvious. Both ROTI and dTEC changed drastically due to the occurrence of magnetic storms, and there were also

many cases of PPP perturbations induced by magnetic storms. ROTI can reach 4 TECU/min, and dTEC fluctuates between -2 TECU and 2 TECU, indicating intense ionospheric fluctuations. In terms of positioning errors, under ionospheric disturbances conditions, the errors ranged from several tens of centimeters to the meter level. For some stations, when ionospheric disturbances were severe, the positioning errors could reach the meter level to the 10 meters magnitude. Moreover, over time, the ionospheric response in this region became more pronounced in 2023 and 2024, which deserves more attention from GNSS users in these areas as the 25th solar cycle approaches its peak.

During magnetic storms, ionospheric disturbances not only directly affect positioning errors but also reduce the ambiguity resolved percentage by disrupting the continuity of carrier phase observations, thereby indirectly impacting the stability of positioning accuracy. Therefore, we recorded the ambiguity data of each station during magnetic storm events, calculated the wide-lane ambiguity resolved percentage (WL_ARP), narrow-lane ambiguity resolved percentage (NL_ARP), and total ambiguity resolved percentage (TL_ARP) respectively, and statistically analyzed the proportions of observational data with success rates exceeding 80% and 60% among the available data of each station. The statistical results are shown in Table 2. It can be observed that under strong magnetic storm conditions, the ambiguity resolved percentage of each station exhibits distinct variations. Among these stations, CHAN demonstrates the most stable performance in ambiguity resolution: the proportion of usable data with WL_ARP exceeding 80% reaches 84.44%, all NL_ARP values are above 80%, and the proportion of usable data with a TL_ARP greater than 80% amounts to 82.22%. Compared with other stations, CHAN achieves the optimal comprehensive performance. The BJFS and BJNM stations, both located in the mid-latitude region, show slightly inferior but still stable ambiguity fixing rates, which are superior to those of other IGS stations. In contrast, stations in the low-to-mid latitude region exhibit a significant degradation in ambiguity fixing performance during magnetic storms. For stations such as CKSV, KMNM, and TCMS, the proportion of usable data with NL_ARP exceeding 80% is extremely low.

.

Table 2 Statistics of ambiguity resolved percentage at each station under the impact of magnetic storm events

Stations	WL_ARP		NL_APR		TL_ARP	
	≥ 80%	≥60%	≥ 80%	≥60%	≥80%	≥60%
BJFS	72.31%	96.92%	83.08%	93.85%	53.85%	80.00%
BJNM	75.00%	100.00%	95.00%	100.00%	60.00%	100.00%
CHAN	84.44%	95.56%	100.00%	100.00%	82.22%	93.33%
URUM	20.00%	89.33%	89.33%	100.00%	13.33%	62.67%
LHAZ	52.38%	82.54%	55.56%	69.84%	42.86%	57.14%
SHAO	20.97%	51.61%	54.84%	54.84%	17.74%	45.16%
WUHN	35.06%	84.42%	63.64%	90.91%	15.58%	54.55%
JFNG	65.38%	92.31%	84.62%	100.00%	34.62%	76.92%
WUH2	29.41%	61.76%	82.35%	100.00%	8.82%	50.00%
HKSL	61.11%	94.44%	52.78%	100.00%	25.00%	72.22%
HKWS	64.71%	94.12%	47.06%	100.00%	23.53%	67.65%
CKSV	47.62%	85.71%	57.14%	95.24%	0.00%	61.90%
KMNM	61.90%	95.24%	66.67%	90.48%	0.00%	71.43%
NCKU	37.50%	50.00%	62.50%	62.50%	37.50%	50.00%
TCMS	59.57%	89.36%	74.47%	100.00%	2.13%	80.85%
TNML	53.49%	86.05%	100.00%	100.00%	37.21%	86.05%
TWTF	52.54%	84.75%	94.92%	96.61%	50.85%	84.75%

3.2 Discussion on Cluster Analysis

The proportion of each station experiencing intense ionospheric disturbances caused by strong geomagnetic storm interference, as well as the proportion of stations with severely impaired positioning accuracy induced by geomagnetic storms, were statistically analyzed. These proportions were correlated with the geographical latitudes of the stations, and dimensional differences were ignored through normalization prior to the conduct of cluster analysis. Figure 6 presents the clustering results of latitude and intense ionospheric disturbance proportion when the number of clusters is set to 2. Figure 7 shows the clustering results of latitude and positioning accuracy disturbance proportion when the number of clusters is set to 2. It can be clearly observed that when the number of clusters is 2, low-latitude stations are grouped into one cluster, while stations in higher-latitude regions are formed into another cluster.

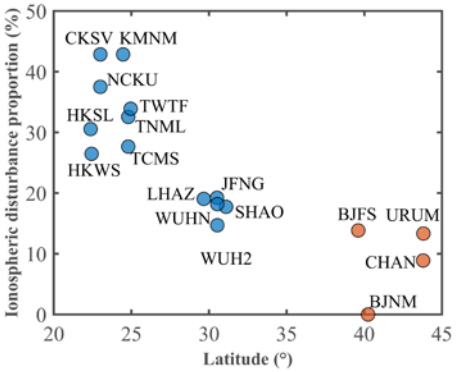

Fig. 6 Cluster analysis of latitude and ionospheric disturbances (k=2)

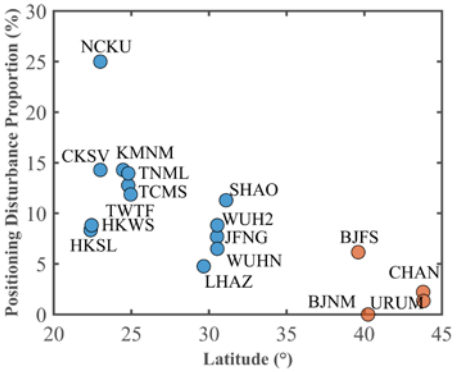

Fig. 7 Cluster analysis of latitude and positioning impacts (k=2)

Fig. 8 presents the clustering results of latitude and intense ionospheric disturbance proportion when the number of clusters is set to 3. Fig. 9 shows the clustering results of latitude and positioning accuracy disturbance proportion when the number of clusters is set to 3. When the number of clusters increases, it can be observed that after eliminating the influence of dimensions, the clustering results show a significant correlation with latitude, and different latitude zones exhibit certain characteristics in their responses to magnetic storms. Stations in low-latitude regions are more severely disturbed by magnetic storms, while the response of PPP in mid-latitude regions to global ionospheric disturbances caused by magnetic storms is relatively weaker compared to that in low-latitude regions.

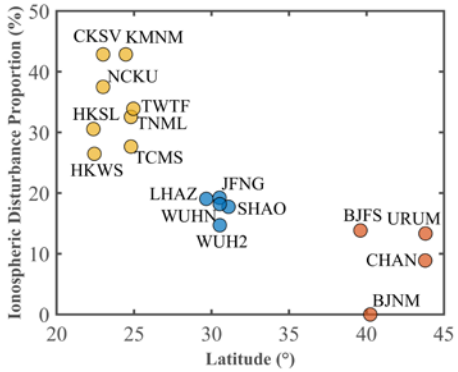

Fig. 8 Cluster analysis of latitude and ionospheric disturbances (k=3)

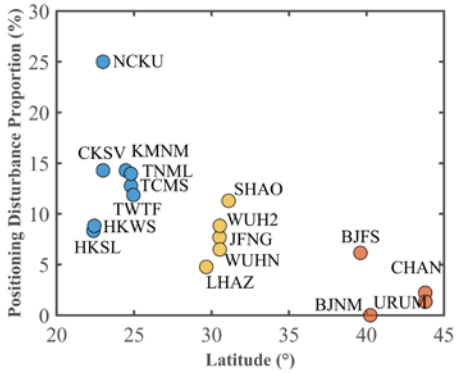

Fig. 9 Cluster analysis of latitude and positioning impacts (k=3)

3.3 Comparison of Positioning Results at Stations with Different Latitudes

From the above experiments, it can be found that the impact of magnetic storms on GPS PPP

shows a significant correlation with the latitude of the station. To further investigate the disturbance of PPP accuracy in China during magnetic storms, we focus on the strong magnetic storm event on December 1, 2023, which caused relatively severe disturbances. Six stations from different mid-low latitude regions in China (namely CHAN, BJFS, WUHN, CKSV, HKWS, and HKSL) are selected as research objects. This magnetic storm was caused by the combined impact of CMEs that erupted on November 27 and 28, 2023. The geomagnetic storm index of this event is shown in Figure 10. The solar wind speed began to increase rapidly at 23:00 on November 30, 2023. Meanwhile, the Dst index dropped rapidly after a slight rise, and the Kp index also started to increase. The minimum Dst index of this magnetic storm event reached -108 nT, with the maximum Kp index reaching 7. From 09:00 to 15:00 UTC on December 1, 2023, the geomagnetic indices peaked, during which the impact of the magnetic storm was the most severe.

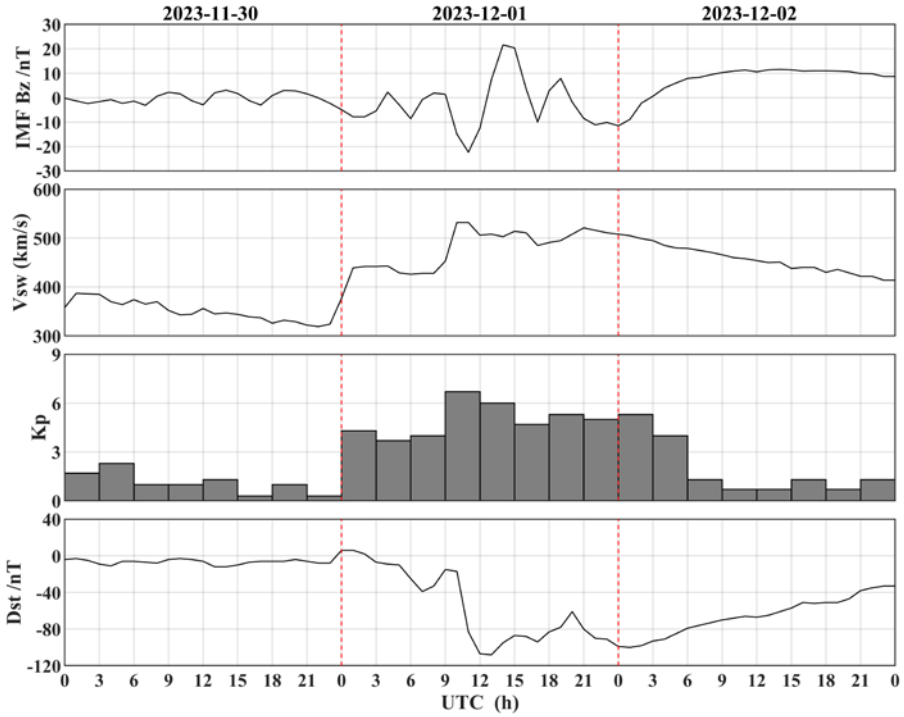

Figure 10 Indices of the magnetic storm

Based on the GNSS observation data from the six stations on December 1, 2023, the ROTI and dTEC indices were calculated, and kinematic PPP was performed using PRIDE PPP-AR.

Figure 11 shows the time variation of the ionospheric dTEC index in the six station areas on the geomagnetic storm day, and Figure 12 displays the time variation of the ionospheric ROTI index. According to the calculation results of ROTI and dTEC, the ionospheric index of the CHAN station fluctuates but remains within the normal range overall. The ionospheric index of the BJFS station begins to show obvious fluctuations. As the latitude continues to decrease, the ionosphere at WUHN, CKSV, HKWS and HKSL stations undergoes severe disturbances. Especially in terms of dTEC, as it gradually enters the main phase of the geomagnetic storm, dTEC can no longer be correctly calculated due to excessive environmental impact. At the same time, the ROTI index also increases rapidly, and the ROTI index at low-latitude stations even reaches 4 TECU/min, indicating that the ionospheric environment in low-latitude regions is severely disturbed by the geomagnetic storm.

Figure 13 shows the time variation diagram of the three-dimensional positioning error of the six stations on the geomagnetic storm day. In this geomagnetic storm event, the CHAN station located

in Changchun was the least affected by the geomagnetic storm compared with other stations, and its positioning remained stable all the time, with the 3D RMS of positioning less than 2 cm. The positioning result of the BJFS station, also in the mid-latitude zone, was relatively stable, with large errors only appearing in individual epochs within an extremely short time. As the latitude decreases, the WUHN station begins to experience frequent positioning disturbances. Entering the low-latitude region, the positioning errors of the three stations increase rapidly, with the maximum error exceeding 10 meters and the RMS reaching the meter level, indicating that the precision of precise point positioning at stations in low-latitude regions of China is more susceptible to geomagnetic storms.

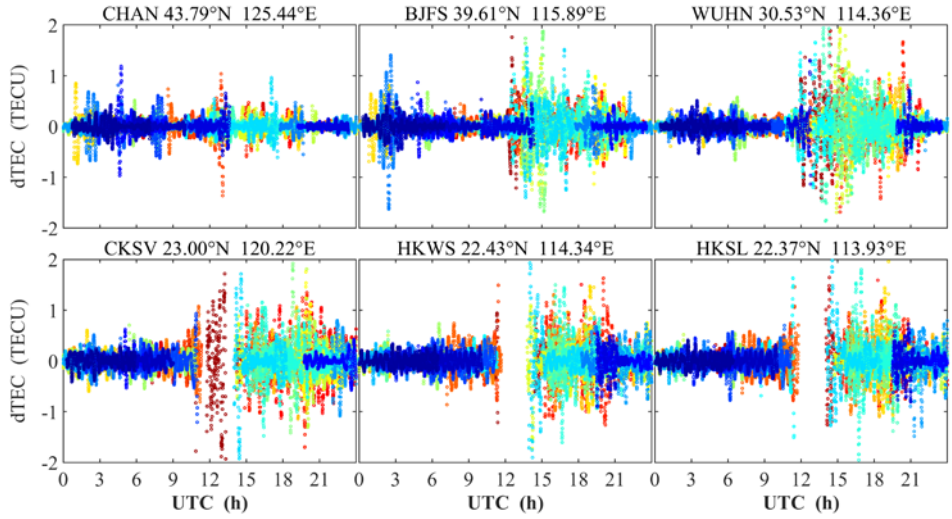

Figure 11 The time series of dTEC of each station on December 1, 2023

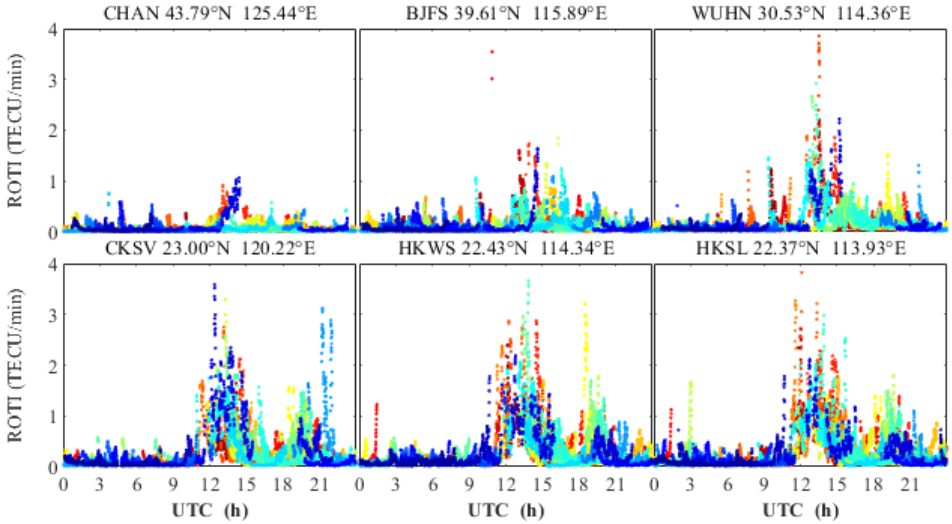

Figure 12 The time series of ROTI of each station on December 1, 2023

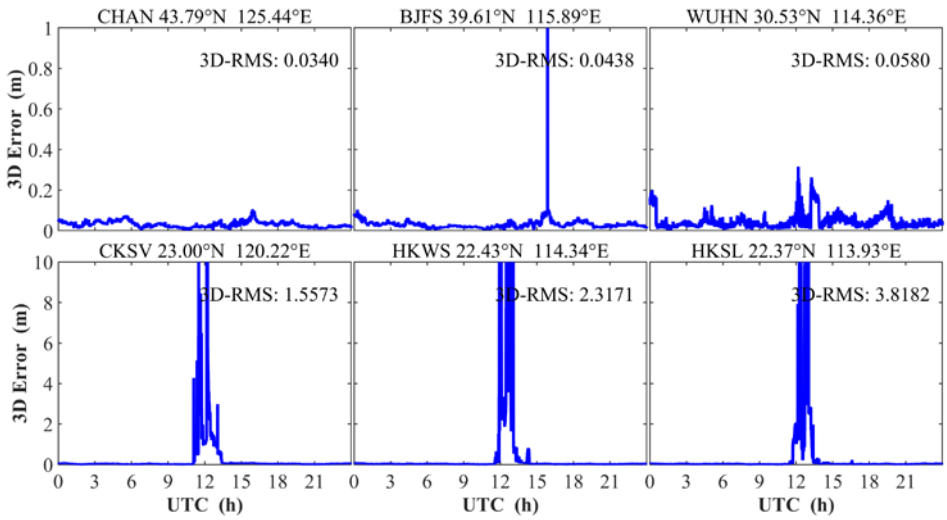

Figure 13 The time series of 3D error of each station on December 1, 2023

4 Conclusions

Using IGS stations datasets in China, this study analyzed the positioning accuracy of PPP during major magnetic storm events from 2000 to 2024 using the PRIDE PPP-AR positioning software. Combined with the ROTI and dTEC indices, the impact of magnetic storms on PPP in the China region was explored. Additionally, stations were selected from different latitude zones to conduct further analysis on the magnetic storm of December 1, 2023. The conclusions are as follows:

1) For the Chinese region, when solved using PRIDE PPP-AR, 50%-60% of strong magnetic storms did not cause significant interference to the ionospheric environment of the stations or the positioning accuracy of PPP.

2) For most regions, approximately 20% of strong magnetic storms induced significant variations in positioning accuracy of GPS PPP.

3) The ionosphere in low-latitude zones of China is more sensitive to magnetic storms and is more severely affected by them. Under intense magnetic storm conditions, the ROTI index can reach 4 TECU/min, the ambiguity resolved percentage decreases significantly, and the 3D error of GNSS PPP can reach several meters.

4) Stations in mid-latitude regions consistently exhibit relatively stable positioning results. Over 90% of magnetic storms did not cause obvious positioning errors, with positioning errors stable at the centimeter level.

Acknowledgements: This study was supported by The National Natural Science Foundation of China (42274042; U25A20397; 42104029), Hunan Provincial Excellent Youth Fund Project (2023JJ20060), and Joint International Research Laboratory of Spatio-temporal Information and Intelligent Location Services (C25GAH02). We would like to thank the IGS for providing the observation data of global tracking stations, and the Satellite Navigation and Positioning Technology Research Center of Wuhan University and the CODE for supplying precise products.

Reference

[1] Zumberge, J. F. ; Heflin, M. B. ; et al.(1997) : Precise point positioning for the efficient and robust analysis of GPS data from large networks[J]. Journal of geophysical research: solid earth, 1997, 102(B3): 5005-5017.

[2] Zhang, X. ; Zuo, X. ;, et al.(2015) : Convergence Time and Positioning Accuracy Comparison between BDS and GPS Precise Point Positioning[J]. Acta Geodaetica et Cartographica Sinica, 2015, 44(3),250-256.

[3] Wang, K. ; Liu, A. ; et al.(2025) : Analysis on open service performance of BDS during peak of solar cycle 25[J]. Journal of Navigation and Positioning, 2025, 13(1): 61-68.

[4] Gonzalez, W. D. ; Joselyn, J. A. ; et al.(1994) What is a geomagnetic storm?[J]. Journal of Geophysical Research: Space Physics, 1994, 99(A4): 5771-5792.

[5] Luo, X. ; Du, J. ; et al.(2022) : ROTI-based stochastic model to improve GNSS precise point positioning under severe geomagnetic storm activity[J]. Space Weather, 2022, 20(7): e2022SW003114.

[6] Polekh, N. ; Zolotukhina, N. ; et al.(2017): Dynamics of ionospheric disturbances during the 17–19 March 2015 geomagnetic storm over East Asia[J]. Advances in Space Research, 2017, 60(11): 2464-2476.

[7] Astafyeva, E. ; Yasyukevich, Y. ; et al.(2014) : Geomagnetic storms, super-storms, and their impacts on GPS-based navigation systems[J]. Space Weather, 2014, 12(7): 508-525.

[8] Luo, X. ; Chen, Z. ; et al.(2023) : Studying the fixing rate of GPS PPP ambiguity resolution under different geomagnetic storm intensities[J]. Space weather, 2023, 21(10): e2023SW003542.

[9] Luo, X. ; Li, Y. ; et al.(2025) : Difference and threshold analysis of scintillation index S4c using GPS data from collocated stations at 30 s intervals during 2010-2023[J]. GPS Solutions, 2025, 29(4), 201

[10] Filjar, R. ; Kos, T. ; et al.(2008) : GPS positioning performance in the wake of the Halloween 2003 geomagnetic storm[C]//2008 50th International Symposium ELMAR. IEEE, 2008, 2: 385-388.

[11] Quan, L. ; Xue, J. ; et al.(2021) : Performance of GPS single frequency standard point positioning in China during the main phase of different classified geomagnetic storms[J]. Chinese Journal of Geophysics (in Chinese), 2021, 64(9): 3030-3047.

[12] Wang, G. ; Wang, N. ; et al.(2021) : Impact of geomagnetic storms on ionosphere variability and precise point positioning application in high latitudes of the northern hemisphere[J]. Chin. J. Space Sci., 202l, 41(2): 261-272.

[13] Sang, W. ; Lou, G. ; et al.(2023) : Ionospheric disturbance monitoring and GNSS positioning performance analysis during geomagnetic storms[J]. GNSS World of China, 2023, 48(5): 71-78.

[14] Zakharenkova, I. ; Cherniak, I. ;(2021) : Effects of storm-induced equatorial plasma bubbles on GPS-based kinematic positioning at equatorial and middle latitudes during the September 7–8, 2017, geomagnetic storm[J]. Gps Solutions, 2021, 25(4): 132.

[15] Li, X. ; Han, J. ; et al.(2023) : A grid-based ionospheric weighted method for PPP-RTK with diverse network scales and ionospheric activity levels[J]. Gps Solutions, 2023,.27, 191.

[16] Zhang, W. ; Zhang, J. ; et al.(2025) : New data processing methods for network RTK positioning: improving ionospheric uncertainty management during ionospheric scintillations[J]. Gps Solutions, 2025, 29, 72.

[17] Li, C. ; Roberts, G. W. ; et al.(2025) : The use of triple-frequency GNSS parameters to monitor ionospheric scintillation in high-latitude regions[J]. Gps Solutions, 2025, 29, 122.

[18] Li, X. ; Wang, B. ; et al.(2025) : Enhancing PPP-RTK performance at low latitudes through mitigation of ionospheric scintillation effects[J]. Gps Solutions, 2025, 29, 143.

[19] Pi, X. ; Mannucci, A. J. ; et al.(1997) : Monitoring of global ionospheric irregularities using the worldwide GPS network[J]. Geophysical Research Letters, 1997, 24(18): 2283-2286.

[20] Cherniak, I. ; Krankowski, A. ; et al.(2018) : ROTI Maps: A new IGS ionospheric product characterizing the ionospheric irregularities occurrence[J]. Gps Solutions, 2018, 22: 1-12.

[21] Tang, L. ; Li, Z. ; et al.(2018) : Large-area tsunami signatures in ionosphere observed by GPS TEC after the 2011 Tohoku earthquake[J]. GPS Solutions, 2018, 22: 1-8.

[22] Geng, J. ; Chen, X. ;et al.(2019) : PRIDE PPP-AR: an open-source software for GPS PPP ambiguity resolution[J]. GPS solutions, 2019, 23: 1-10.

[23] Geng, J. ; Wen, Q. ; et al.(2022) : GNSS observable-specific phase biases for all-frequency PPP ambiguity resolution[J]. Journal of Geodesy, 2022, 96(2): 11.

Authors

Wei Xiang is currently a graduate student at the School of Geography and Information Engineering, China University of Geosciences (Wuhan), located in Wuhan, China. His research focuses on precise point positioning during magnetic storms.

Xiaomin Luo is currently an associate professor at the School of Geography and Information Engineering, China University of Geosciences (Wuhan). He received his Ph.D. degree from the GNSS research center of Wuhan University in 2020. His current research mainly focuses on GNSS ionospheric scintillation and GNSS PPP.

Zhuang Chen is currently a doctoral student at Wuhan University, located in Wuhan, China. His research focuses on the algorithm analysis, performance evaluation and accuracy improvement of multi-system precise point positioning under geomagnetic storm conditions.

Biyan Chen is currently an associate professor at Central South University. He received his Ph.D. degree from the Hong Kong Polytechnic University in 2017. His research interests include GNSS meteorology, water vapor tomography, extreme weather forecasting, and seismo-ionospheric anomalies.

Ankang Xie is currently a graduate student at the School of Geography and Information Engineering, China University of Geosciences (Wuhan), located in Wuhan, China. His research interests are RTK positioning calculation in complex ionospheric environments.

Lingqiao Zeng is currently a graduate student at the School of Geography and Information Engineering, China University of Geosciences (Wuhan), located in Wuhan, China. His research focuses on the impact and improvement of precise positioning under ionospheric irregularities in low-latitude regions.

Yingrui Wang is currently an undergraduate student at the School of Geography and Information Engineering, China University of Geosciences (Wuhan), located in Wuhan, China. Her research focuses on the impact of magnetic storm on precision positioning.

Kamarul Hawari Bin Ghazali, Prof. Ir. Dr., is a senior academic and researcher at Universiti Malaysia Pahang Al-Sultan Abdullah (UMPSA), specializing in artificial intelligence, deep learning, machine vision, data analytics, and GNSS signal processing.